Ecological Informatics xxx (xxxx) xxx-xxx

Contents lists available at ScienceDirect

Ecological Informatics

journal homepage: http://ees.elsevier.com

# Performance of four state-of-the-art GPP products (VPM, MOD17, BESS and PML) for grasslands in drought years

Yanyan Pei [a], Jinwei Dong [a,*], Yao Zhang [c], Jilin Yang [a,b], Yongqiang Zhang [d], Chongya Jiang [e], Xiangming Xiao [b]

[a] Key Laboratory of Land Surface Pattern and Simulation, Institute of Geographic Sciences and Natural Resources Research, CAS, Beijing 100101, China
[b] Department of Microbiology and Plant Biology, Center for Spatial Analysis, University of Oklahoma, Norman, OK 73019, USA
[c] Department of Earth and Environmental Engineering, Columbia University, New York, NY 10027, USA
[d] Key Laboratory of Water Cycle and Related Land Surface Processes, Institute of Geographic Sciences and Natural Resources Research, Chinese Academy of Sciences, CAS, Beijing 100101, China
[e] Department of Landscape Architecture and Rural Systems Engineering, Seoul National University, South Korea

ARTICLE INFO

*Keywords*
Gross primary production (GPP)
Drought
VPM
BESS
PML
MOD17
Light use efficiency model
Process-based model

ABSTRACT

Accurate estimation of gross primary production (GPP) is of significance for understanding the changes of carbon uptake and its responses to extreme climate events like droughts. Emerging new GPP products with higher spatial and temporal resolutions (500-1000 m, 8-day) from the Moderate Resolution Imaging Spectroradiometer (MODIS) Photosynthesis (MOD17), the Vegetation Photosynthesis Model (VPM), the Breathing Earth System Simulator (BESS), and the Penman-Monteith-Leuning (PML) models, provided unprecedented opportunities to understand the spatial and temporal variations of GPP. However, their performances under drought conditions remain obscure. Here we evaluated the performance of these four state-of-the-art GPP products in grasslands, using FLUXNET data as reference. The results showed that all the four models have reasonable accuracies under non-drought years. In drought years, the VPM performed best, followed by the MOD17, PML and BESS, with the RMSEs of 1.67, 1.69, 1.72 and 1.77 gC $m^{-2}$ $day^{-1}$, respectively. The VPM, BESS and PML overestimated annual GPP by 2%, 13% and 21%, respectively, while MOD17 underestimated annual GPP by 10% in drought years. This varied model performances under drought years could be partially attributed to the differences in quantifying the water stress effects. The water constraint factor in the VPM, which is derived from the Land Surface Water Index (LSWI) and directly indicates the overall water content of leaf, plant stand and soil background, could better capture the vegetation response to water content variation than that in MOD17, PML and BESS, all of which used an atmospheric moisture related indicator (the Vapor Pressure Deficit for MOD17 and PML, and the relative humidity for BESS). This study suggests that water stress factors, which reflect the physiological and ecological characteristics of vegetation itself (e.g., LSWI) rather than atmospheric moisture (e.g., VPD) or other meteorological surrogates, should be further considered in GPP models when applied in drought conditions

## 1. Introduction

Gross primary production (GPP) of terrestrial vegetation is known as the largest carbon fluxes in terrestrial carbon cycle (Beer et al., 2010; Zhang et al., 2016b). Accurate estimation of GPP is required for understanding the changes of global carbon cycle and quantifying the responses of terrestrial ecosystem to climate change (Ryu et al., 2019; Stocker et al., 2019). However, the extreme climate events, such as severe droughts, can lead to vegetation stomatal closure and photosynthetic rate decline, thus resulting in vegetation growth reduction and even mortality, and finally impose a reduction in terrestrial ecosystem productivity (He et al., 2018;

* Corresponding author at: Institute of Geographic Sciences and Natural Resources Research, Chinese Academy of Sciences, 11A, Datun Road, Chaoyang District, Beijing 100101, China.
*E-mail addresses:* peiyy@igsnrr.ac.cn (Y. Pei); dongjw@igsnrr.ac.cn (J. Dong)

https://doi.org/10.1016/j.ecoinf.2020.101052
Received 23 September 2019; Received in revised form 11 December 2019; Accepted 1 January 2020
Available online xxx
1574-9541/

Stocker et al., 2019; Wolf et al., 2016). By resolving the systematic biases in GPP estimation under droughts for remote sensing-based models (RS models) (i.e., Moderate Resolution Imaging Spectroradiometer (MODIS) Photosynthesis, MOD17; the Vegetation Photosynthesis Model, VPM; the Breathing Earth System Simulator, BESS; and P model), Stocker et al. (2019) found that the global GPP had on average reduced by 15% due to droughts as indicated by soil moisture stress, and the reduction of GPP was even higher (~50%) in semi-arid grasslands and savannahs (Stocker et al., 2019). Yu et al. (2017) also reported that the drought-induced MOD17 GPP reduction was 48% in the mid-latitude region of the Northern Hemisphere and 13% in the low-latitude region of the Southern Hemisphere compared to normal period (Yu et al., 2017). The accurate estimation of GPP under drought conditions is vital for understanding the impacts of droughts on carbon cycle dynamics (Angert et al., 2005; Mishra and Singh, 2010; Wolf et al., 2016), plant recovery from droughts (He et al., 2018; Schwalm et al., 2017), and spatiotemporal patterns of changes in regional and global GPP (Angert et al., 2005; Chen et al., 2017; Yao et al., 2018; Zhang et al., 2016c).

Remote sensing-based GPP models are widely used for estimating vegetation GPP across the site, regional and global scales (Ryu et al., 2019). Recently, there are four state-of-the-art global GPP products with higher spatial and temporal resolutions (500-1000 m, 8-day) (Jiang and Ryu, 2016; Running and Zhao, 2015; Zhang et al., 2017; Zhang et al., 2019b). Two of them are derived from light use efficiency (LUE) models including MOD17 (Running et al., 2004) and VPM (Xiao et al., 2004a; Xiao et al., 2004b), and the other two are process-based models like BESS (Ryu et al., 2011) and the Penman-Monteith-Leuning (PML) model (Leuning et al., 2008; Zhang et al., 2010). These GPP products provide unprecedented opportunities to document spatial patterns and temporal dynamic changes of GPP for the global terrestrial ecosystems (Jiang and Ryu, 2016; Running and Zhao, 2015; Zhang et al., 2017; Zhang et al., 2019b). However, previous studies that included these products have shown that there are large differences among these products in estimating terrestrial ecosystem GPP. For example, the global annual GPP from the four data products ranged from 110 to 146 PgC $year^{-1}$, with the annual increasing trend ranging from 0.20 to 0.39 PgC $year^{-1}$ and the coefficient of determination ($R^2$) between GPPs from these four products and eddy covariance flux tower sites ($GPP_{EC}$) varying from 0.59 to 0.73 (Jiang and Ryu, 2016; Running and Zhao, 2015; Zhang et al., 2017; Zhang et al., 2019b). In details, Indonesia witnessed the opposite trends derived from two products (i.e., BESS and MOD17) that the BESS showed positive changes, while the MOD17 displayed negative changes (Jiang and Ryu, 2016).

Under drought, there is a common bias of GPP estimated from theses RS GPP products (e.g., MOD17, BESS, and VPM), and the bias increases during the course of droughts (Sjostrom et al., 2013; Stocker et al., 2019; Wu et al., 2018). On the contrary, the performance of PML GPP product under drought has not been studied yet (Zhang et al., 2019b). The bias existing in these GPP estimates under drought may be rooted in their different ways to resolve dryness effects (Stocker et al., 2019). For example, MOD17 and PML uses vapor pressure deficit (VPD) as a surrogate of moisture stress (Coops et al., 2007; Nightingale et al., 2007; Zhang et al., 2019b; Zhao et al., 2005; Zhu et al., 2018). BESS uses relative humidity (RH) via Ball-Berry model to consider the water stress effect on canopy conductance (Ball, 1988; Ryu et al., 2011). Both VPD and RH are atmosphere moisture related indexes. While VPM uses satellite-based land surface water index (LSWI) to account for water constraint (Dong et al., 2015; Doughty et al., 2018; Wagle et al., 2014; Wagle et al., 2015; Xiao et al., 2004a; Xiao et al., 2004b; Zhang et al., 2017), which is a plant moisture related index. Moreover, previous studies have demonstrated that LUE was more sensitive to plant moisture indicators (such as LSWI) than atmospheric moisture indicators (such as VPD) in comprehensive situations (Zhang et al., 2015). However, the sensitivity of these moisture indices to drought remains unknown. To study which kind of moisture indicators can better capture the response of plant to drought is of great significance for improvement of GPP models and thus accurate estimating of GPP in water-limited areas or plants.

Moreover, there is a lack of consistency assessment of these four emerging GPP products using the same criteria, especially under drought for specific ecosystems, such as grasslands. Grasslands are more susceptible to drought stress since they have less accessibility to soil water with shallower roots compared to forests (Frank et al., 2015; Wu et al., 2018). However, grasslands actually have the similar amounts of carbon stocks with forests globally, because grasslands are more geographically distributed.(Hoover and Rogers, 2016). Previous studies have shown that grasslands in the US often act as carbon sinks, whereas they can become carbon sources during drought(Zhang et al., 2011). The study of grasslands carbon dynamics under drought is of great significance for understanding the potential feedbacks to climate change, which requires reliable GPP products to provide high accurate data. Therefore, it is essential to evaluate the performances of these four state-of-the-art GPP products under drought for grasslands, which can provide some references for the selection of products in future studies.

The objectives of this study are: 1) to conduct a comprehensive evaluation of these four GPP products, as well as exploring the differences between the LUE models and the process-based models in their performances under drought years; and 2) to explore the sensitivity of plant moisture indicator and atmospheric moisture indicator in response to drought. In this study, we used $GPP_{EC}$ to evaluate the performances of these four GPP products under drought years. To achieve these aims, we firstly describe the major characteristics of the climate, GPP and vegetation indices in drought and non-drought years. Then, we compare the 8-day and annual sum GPP from the four GPP products with that from the flux tower sites in drought and non-drought years. Thirdly, we conduct a comparison between the LUE models and the process-based models, as well as the comparison within LUE/process-based models (i.e., VPM vs. MOD17, and BESS vs. PML). The results are expected to contribute to the improvement of the current GPP models and their applications in grassland ecosystem, especially under severe drought years.

## 2. Materials and methods

### *2.1. Reference GPP data from $CO_2$ eddy flux towers*

Eddy covariance flux tower sites provide landscape-scale measurements of ecosystem carbon fluxes, including net ecosystem $CO_2$ exchange (NEE) (Baldocchi et al., 2001). The observed NEE was partitioned into GPP and ecosystem respiration ($R_e$) based on the nighttime method (Reichstein et al., 2005). 51 site-years of data from 9 grassland flux towers (Table 1) at the daily scale in the FLUXNET 2015 web-

**Table 1**
The information of grassland FLUXNET sites used in the study.

| Site ID | Longitude | Latitude | Year range | Citation |
|---|---|---|---|---|
| US-AR1 | 99.42 W | 36.4267 N | 2009–2012 | (Baldocchi and Penuelas, 2019) |
| US-AR2 | 99.5975 W | 36.6358 N | 2009–2014 | (Baldocchi and Penuelas, 2019) |
| US-ARb | 98.0402 W | 35.5497 N | 2005–2006 | (Fischer et al., 2012; Wagle et al., 2014) |
| US-ARc | 98.04 W | 35.5465 N | 2005–2006 | (Fischer et al., 2012; Wagle et al., 2014) |
| US-Goo | 89.8735 W | 34.2547 N | 2002–2006 | http://sites.fluxdata.org/US-Goo/ |
| US-IB2 | 88.241 W | 41.8406 N | 2004–2011 | (Wagle et al., 2014) |
| US-SRG | 110.8277 W | 31.7894 N | 2008–2014 | (Bhattarai et al., 2018; He et al., 2018) |
| US-Var | 120.9507 W | 38.4133 N | 2000–2014 | (Baldocchi and Penuelas, 2019; Chu et al., 2018) |
| US-Wkg | 109.9419 W | 31.7365 N | 2004–2014 | (He et al., 2018; Scott et al., 2010; Wolf et al., 2016) |

site (http://www.fluxdata.org) were used for the validation. These sites were selected because they have at least two years' observations and include at least one drought year (Fig. 1, Section 2.3). The meteorological data, including air temperature, precipitation, VPD, and short-wave solar radiation, observed at the selected flux sites, were used in this study to describe the characteristics of the flux sites in drought and non-drought years. Then the daily $GPP_{EC}$ and meteorological data were all averaged to 8-day mean data to match the temporal resolution of the modeled GPPs (i.e., $GPP_{MOD17}$, $GPP_{VPM}$, $GPP_{BESS}$, and $GPP_{PML}$).

### *2.2. The global GPP data products*

#### *2.2.1. MOD17 GPP data product*

The MODIS standard product (MOD17) uses the concept of the light use efficiency (Monteith, 1972), which estimate GPP as the product of the incident photosynthetically active radiation (PAR), the fraction of absorbed photosynthetically active radiation (FPAR) by plants and the actual LUE ($\varepsilon$) of vegetation (Monteith, 1972). The MOD17 algorithm is shown as follows:

$$GPP_{MOD17} = APAR \times \varepsilon \tag{1}$$

where APAR is the absorbed photosynthetically active radiation, and $\varepsilon$ is the actual light use efficiency (LUE).

In the MOD17 algorithm, the $\varepsilon$ is derived from the attenuation of its maximum value ($\varepsilon_{max}$) by two environmental stresses: (1) the minimum temperature, which may inhibit the photosynthesis by reducing enzyme activity, and (2) the VPD, as that high atmospheric VPD may reduce the stomatal conductance (Prince and Goward, 1995; Running et al., 2004; Running and Zhao, 2015; Zhao et al., 2005).

$$\varepsilon = \varepsilon_{\max} \times TMIN_{scalar} \times VPD_{scalar} \tag{2}$$

where $\varepsilon_{max}$ is the maximum light use efficiency, which is optimized in advance and given in a Biome Parameter Look-up Table (BPLUT) for each land cover type. $TMIN_{scalar}$

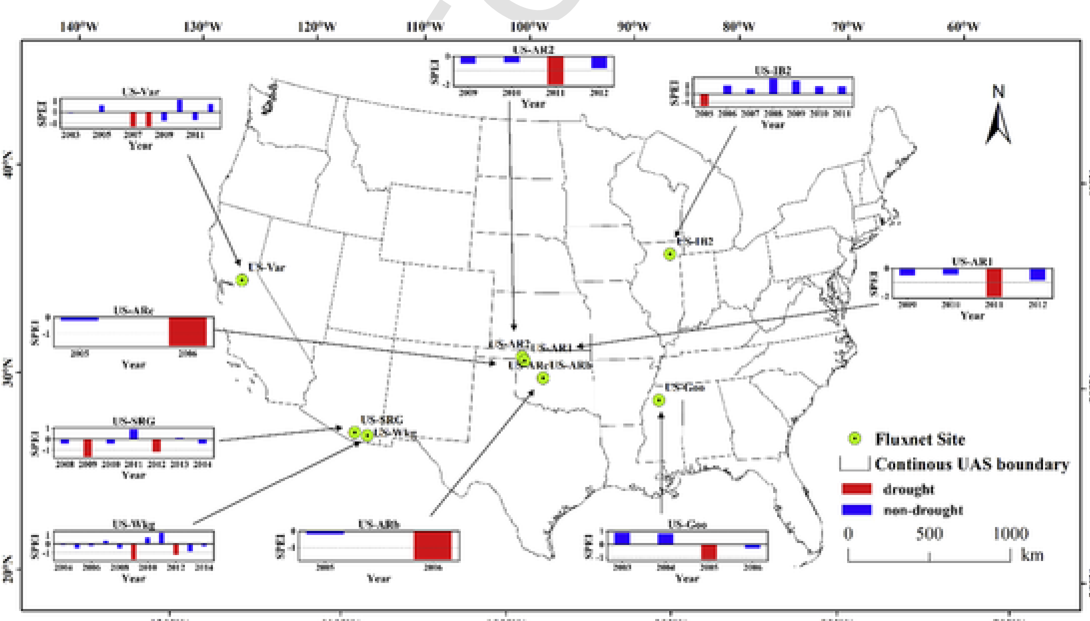


**Fig. 1.** The Standardized Precipitation-Evapotranspiration Index (SPEI) for the 9 grassland FLUXNET sites and the identification of the drought years.

and $VPD_{scalar}$ are environmental stress factors and parameterized according to Eqs. (3) and (4):

$$TMIN_{scalar} = \begin{cases} 1 \; TMIN > TMIN_{\max} \\ \left(TMIN - TMIN_{\min}\right) / \left(TMIN_{\max} - TMIN_{\min}\right) \; TMIN_{\mathrm{mi}} \\ 0 \; TMIN < TMIN_{\min} \end{cases}$$

$$VPD_{scalar} = \begin{cases} 0 \; VPD > VPD_{\max} \\ \left(VPD_{\max} - VPD\right) / \left(VPD_{\max} - VPD_{\min}\right) \; VPD_{\min} \leq VP \\ 1 \; VPD < VPD_{\min} \end{cases}$$

where TMIN and VPD are the daily minimum temperature (°C) and average VPD (Pa), $TMIN_{max}$ and $VPD_{max}$ are the daily maximum temperature and average VPD at which $\varepsilon = \varepsilon_{max}$, and $TMIN_{min}$ and $VPD_{min}$ are the daily minimum temperature and average VPD at which $\varepsilon = 0$. These parameters were determined for each land cover type in the BPLUT.

#### 2.2.2. VPM GPP data product

The VPM model estimates the GPP as the products of $APAR_{chl}$ and $\varepsilon$ (Xiao et al., 2004a; Xiao et al., 2004b):

$$GPP_{VPM} = \varepsilon \times APAR_{chl} \tag{5}$$

where $APAR_{chl}$ is the absorbed photosynthetically active radiation by chlorophyll, and $\varepsilon$ is the actual light use efficiency (LUE).

$APAR_{chl}$ is estimated as follows:

$$APAR_{chl} = PAR \times FPAR_{chl} \tag{6}$$

$$FPAR_{chl} = (EVI - 0.1) \times 1.25 \tag{7}$$

where $APAR_{chl}$ is the absorbed photosynthetically active radiation by chlorophyll, PAR is the photosynthetically active radiation, EVI is the Enhanced Vegetation Index (EVI) and $FPAR_{chl}$ is the fraction of PAR absorbed by chlorophyll, which is a linear function of EVI.

The ε is down-regulated by temperature stress ($T_{scalar}$) and water stress ($W_{scalar}$) factors from its maximum value ($\varepsilon_{max}$).

$$\varepsilon = \varepsilon_{max} \times T_{scalar} \times W_{scalar} \tag{8}$$

$$T_{scalar} = \frac{\left(T - T_{min}\right)\left(T - T_{max}\right)}{\left(T - T_{min}\right)\left(T - T_{max}\right) - \left(T - T_{opt}\right)^2} \tag{9}$$

$$W_{scalar} = \frac{1 + LSWI}{1 + LSWI_{max}} \tag{10}$$

where $\varepsilon_{max}$ is the maximum light use efficiency (g C mol$^{-1}$ APAR), which only differs by C3/C4 photosynthesis pathways in the VPM GPP products. Both $T_{scalar}$ and $W_{scalar}$ are ranging from 0 to 1. $T_{min}$, $T_{max}$, and $T_{opt}$ represent the minimum, maximum, and optimum temperatures for photosynthetic activities, respectively. In the VPM GPP product, the $T_{min}$, $T_{max}$, and $T_{opt}$ were set as 0°C, 48°C, and 27°C for grassland, respectively. $W_{scalar}$ is estimated based on the LSWI derived from MODIS data. $LSWI_{max}$ is the maximum LSWI during the snow-free period for each pixel each year. More details about the VPM model and VPM GPP product can be found in Xiao et al. (2004a, 2004b) and Zhang et al. (2017).

#### 2.2.3. BESS GPP data product

BESS is a sophisticated process-based model and driven by several modules, including: (1) atmospheric radiative transfer, which is based on an atmospheric radiative transfer model (Forest Light Environmental Simulator, FLiES) with the input variables of solar zenith angle, aerosol optical thickness, land surface albedo, cloud top height, atmospheric profile type, aerosol type, cloud type (Ryu et al., 2018); (2) canopy radiative transfer, which uses different methods to quantify APAR, near-infrared radiation (NIR), longwave radiation, and net radiation for sunlit and shaded leaves; (3) canopy photosynthesis, which considers the biochemical photosynthesis pathways for C3 and C4 plants based on Farquhar model(Collatz et al., 1992; Farquhar et al., 1980); (4) maximum carboxylation rate ($V_{cmax}$), which is plant functional types (PFT) dependent peak values down-regulated by seasonal LAI variations; (5) two-leaf canopy conductance and temperature, which uses the Ball-Berry equation (Ball et al., 1987) and the analytic solution of leaf energy balance to calculate the two-leaf canopy conductance and temperature, respectively; and (6) evapotranspiration, which is based on the Penman-Monteith equation (Jiang and Ryu, 2016; Ryu et al., 2011).

The global BESS GPP product was generated from this process-based model. It provides GPP data with the spatial resolution of 1 km and temporal resolution of 8-day from 2001 to 2015 (http://environment.snu.ac.kr/bess/) (Jiang and Ryu, 2016; Ryu et al., 2011).

#### 2.2.4. PML GPP data product

The PML model was first developed by Leuning et al. (2008) (Leuning et al., 2008) through introducing a biophysical model for surface conductance ($G_s$) based on Penman-Monteith (PM) equation. Since then there are two improved versions of the PML model (PML-V1 and PML—V2) (Gan et al., 2018; Zhang et al., 2016a). PML-V2 used a biophysical canopy conductance ($G_c$) model to couple ET with GPP (Gan et al., 2018). Zhang et al. (2019a, 2019b) further improved the PML-V2 by incorporating the VPD to constraint GPP as follows (Zhang et al., 2019b):

$$GPP_{PML} = f\,(\mathrm{VPD})\,A \tag{11}$$

$$f\,(\mathrm{VPD}) = \begin{cases} 1, VPD \leq VPD_{\min} \\ \frac{VPD_{\max} - VPD}{VPD_{\max} - VPD_{\min}}, VPD_{\min} < VPD < VPD_{\max} \\ 0, VPD \geq VPD_{\max} \end{cases} \tag{12}$$

where $A$ is the gross assimilation rate, and $f$(VPD) is the VPD constraint function. $VPD_{max}$ is the threshold above which there is no assimilation, and $VPD_{min}$ is the threshold below which there is no vapor pressure constraint.

### 2.3. Climate data and identifying drought years

We used the Standardized Precipitation-Evapotranspiration Index (SPEI) drought index to identify the drought years for the 9 grassland sites (Fig. 1). The effects of precipitation and temperature on drought were considered simultaneous in the SPEI, which was estimated by integrating both the climatic water balance and cumulative water deficit into account (Naumann et al., 2014; Um et al., 2018; Vicente-Serrano et al., 2010; Vicente-Serrano et al., 2015). The SPEI data was derived from the SPEI base v2.5 (Vicente-Serrano et al., 2010). We selected the SPEI data sets with the time scale of 12 months to recognize the drought years. The drought years were defined as SPEI $< -1.00$ according to previous studies (Potop et al., 2014; Prabnakorn et al., 2018).

### *2.4. Statistical analysis of model performance in drought and non-drought years*

The GPPs from the four models ($GPP_{MOD17}$, $GPP_{VPM}$, $GPP_{BESS}$, and $GPP_{PML}$) were evaluated against the $GPP_{EC}$. Firstly, the drought years were extracted for each site using SPEI. Secondly, the linear regression method was used to analyze the relationships between the $GPP_{EC}$ and the GPPs estimated from the four models. The coefficient of determination ($R^2$), Root Mean Squared Error (RMSE)(Cote et al., 2018), Nash-Sutcliffe Efficiency (NSE) and Bias (Eq. (18)) between the $GPP_{EC}$ and the predicted GPPs were calculated in drought and non-drought years, respectively. Thirdly, the annual sum GPP from the four models were compared with that from the flux tower sites to assess the overestimation or underestimation of the four GPP models in annual GPP.

$$RMSE = \sqrt{\sum_{n=1}^{N} \left(GPP_n^{modeled} - GPP_n^{EC}\right)^2 / N} \tag{13}$$

$$\text{NSE} = 1 - \frac{\sum_{n=1}^{N} \left|GPP_n^{modeled} - GPP_n^{EC}\right|^2}{\sum_{n=1}^{N} \left|GPP_n^{modeled} - \overline{GPP^{EC}}\right|^2} \tag{14}$$

$$\text{Bias} = \frac{GPP_{modeled} - GPP_{EC}}{GPP_{EC}} \times 100\% \tag{15}$$

where $N$ is the number of observations; $GPP_n^{EC}$, $\overline{GPP^{EC}}$ are the $n^{th}$ and average $GPP_{EC}$, respectively. $GPP_n^{modeled}$ is the $n^{th}$ corresponding estimated GPP from the four models.

### *2.5. Other auxiliary materials*

We also used several spectral indices in this study. Three vegetation indices, including Normalized Differential Vegetation Index (NDVI), EVI, and LSWI, were calculated for each site, by using the MODIS 8-day composite surface reflectance data (MOD09A1). These indices were compared with $GPP_{EC}$ to further illustrate the major characteristics of vegetation growth in drought years and non-drought years. While the GPP values were simulated and could be biased due to parameterization, spectral indices (NDVI, EVI, and LSWI) can be observed as independent reference. These remote sensing indices were calculated as follows:

$$\text{NDVI} = \frac{\rho_{NIR} - \rho_{Red}}{\rho_{NIR} + \rho_{Red}} \tag{16}$$

$$\text{EVI} = 2.5 \times \frac{\rho_{NIR} - \rho_{Red}}{\rho_{NIR} + 6 \times \rho_{Red} - 7.5 \times \rho_{Blue} + 1} \tag{17}$$

$$\text{LSWI} = \frac{\rho_{NIR} - \rho_{SWIR}}{\rho_{NIR} + \rho_{SWIR}} \tag{18}$$

where $\rho_{NIR}$, $\rho_{Red}$, $\rho_{Blue}$, and $\rho_{SWIR}$ are the surface reflectance values of near infrared band (841–875 nm), red band (620–670 nm), blue band (459–479 nm) and shortwave infrared band (1628–1652 nm), respectively.

## 3. Results

### *3.1. Major characteristics of climate, GPP and vegetation indices in drought years*

The drought index SPEI was used to identify the drought years. A total of 12 drought site-years were identified by SPEI (SPEI $< -1.00$) (Fig. 1).

In those drought years, the VPD and temperature showed larger values, while the $GPP_{EC}$, EVI, LSWI, and precipitation showed smaller values than that in non-drought years (Figs. 2 and 3). For example, at the US-AR1 site, the annual average VPD and temperature in drought years increased by 40% and 4% compared to the non-drought years, while the $GPP_{EC}$, EVI, LSWI and precipitation decreased by 74%, 18%, 67%, and 42%, respectively. The same phenomenon also occurred in the site of US-AR2, US-ARb, US-ARc, US-Goo, US-SRG in 2009, and US-Var in 2008. At US-IB2 site, the annual average VPD and temperature increased by 26% and 11% in drought years, while the EVI, LSWI and precipitation decreased by 18%, 12%, and 47%, respectively.

### *3.2. Comparison of four modeled GPP products ($GPP_{MOD17}$, $GPP_{VPM}$, $GPP_{BESS}$, and $GPP_{PML}$) in drought and non-drought years*

In general, all the four models performed well in predicting GPP, with $R^2 \geq 0.46$, RMSE$\leq$2.23 $gCm^{-2}$ $day^{-1}$, and NSE $\geq 0.42$, and $GPP_{VPM}$ performed best among the four GPP models, with $R^2 = 0.59$, RMSE $= 1.98$ $gCm^{-2}$ $day^{-1}$, and NSE $= 0.54$ (Fig. 4). The estimation accuracies of GPP in the non-drought years were higher than that in drought years for all the four models, with the $R^2 \geq 0.58$ (0.52), RMSE$\leq$2.08 (1.77) $gCm^{-2}$ $day^{-1}$, and NSE $\geq 0.56$ (0.47) in non-drought (drought) years (Fig. 4). In non-drought years, $GPP_{VPM}$ had the highest $R^2$ (0.73) and NSE (0.72) and lowest RMSE (1.66 $gCm^{-2}$ $day^{-1}$), $GPP_{BESS}$ ($R^2 = 0.68$, RMSE $= 1.75$ $gCm^{-2}$ $day^{-1}$ and NSE $= 0.68$) and $GPP_{PML}$ ($R^2 = 0.68$, RMSE $= 1.81$ $gCm^{-2}$ $day^{-1}$, and NSE $= 0.66$) had the similar performances, whereas $GPP_{MOD17}$ had the lowest $R^2$ (0.58) and NSE (0.56) and the highest RMSE (2.08 $gCm^{-2}$ $day^{-1}$) among the four models (Fig. 4). In drought years, however, $GPP_{VPM}$ and $GPP_{MOD17}$ performed better than $GPP_{PML}$ and $GPP_{BESS}$, and the accuracy ($R^2$, RMSE, and NSE) of GPP declined larger in BESS and smaller in MODIS compared to that in non-drought years.

For individual site, all the four models performed well in predicting the $GPP_{EC}$. $GPP_{VPM}$ had the highest $R^2$, NSE, and lowest RMSE among the four models in general. Moreover, all the four models performed better in non-drought years than that in drought years for most of the sites, with the $R^2$ and NSE higher and RMSE lower in non-drought years. In non-drought years, $GPP_{VPM}$ ($R^2$ 0.49–0.94, RMSE 0.72–2.36 $gCm^{-2}$ $day^{-1}$, NSE 0.49–0.89) performed best among the four models, $GPP_{BESS}$ ($R^2$ 0.37–0.80, RMSE 0.71–3.49 $gCm^{-2}$ $day^{-1}$, NSE 0.27–0.80) came second, and $GPP_{PML}$ and $GPP_{MOD17}$ didn't performed as well as the earlier two models (Fig. 6). In drought years, $GPP_{VPM}$ had the highest $R^2$, NSE and lowest RMSE in most of the sites, such as US-ARb, US-ARc, US-SRG (Fig. 6). $GPP_{MOD17}$ performed best in US-AR2 and US-Goo. $GPP_{PML}$ performed best both in US-IB2 and US-Var (Fig. 6), while $GPP_{BESS}$ performed not as well as other models in drought years.

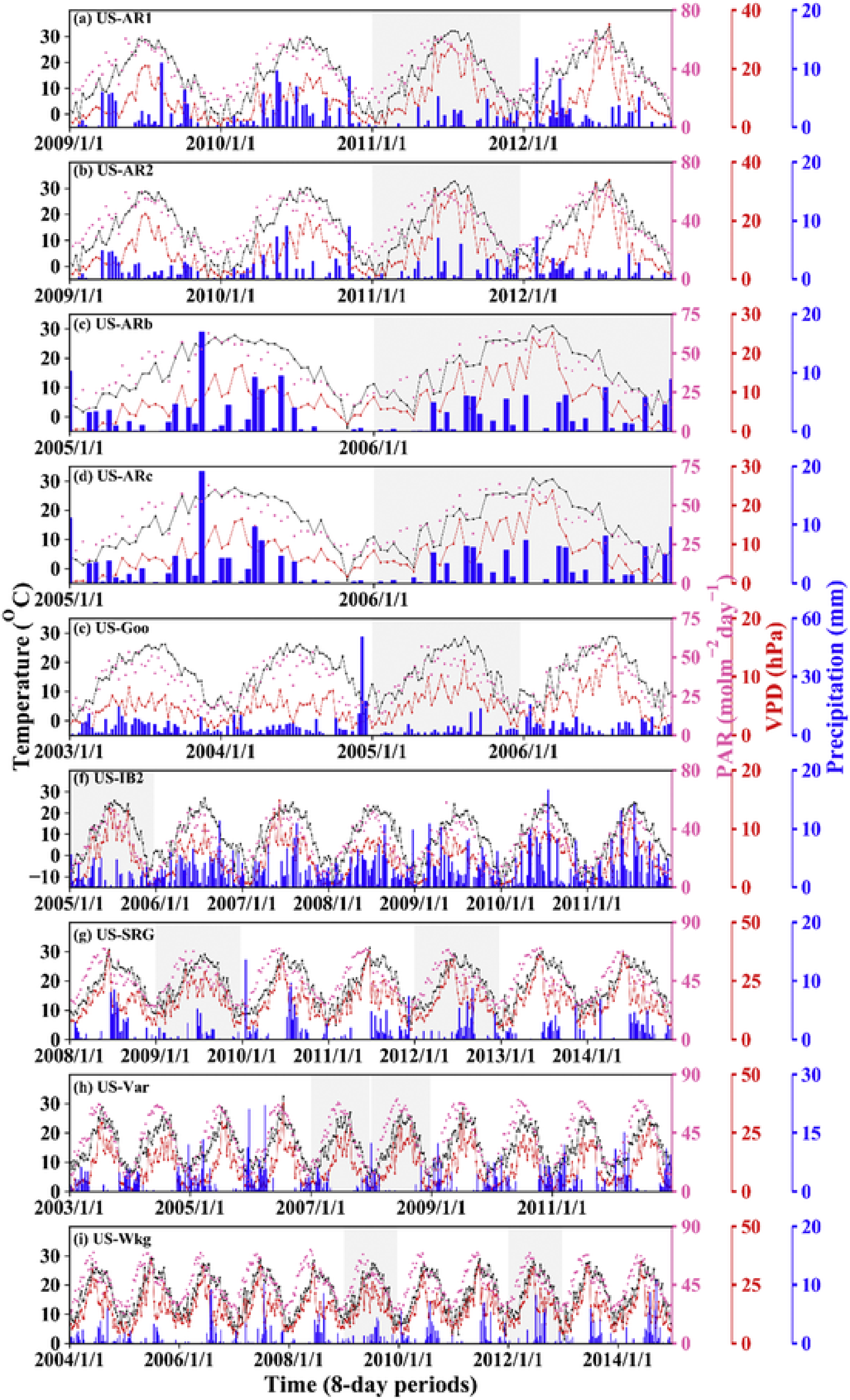
(a) US-AR1
(b) US-AR2
(c) US-ARb
(d) US-ARc
(e) US-Goo
(f) US-IB2
(g) US-SRG
(h) US-Var
(i) US-Wkg
Temperature (°C)
PAR (molm−2 day−1)
VPD (hPa)
Precipitation (mm)
Time (8-day periods)

**Fig. 2.** Annual dynamics and interannual variations of temperature, precipitation, photosynthetically active radiation (PAR), and vapor pressure deficit (VPD) with an interval of 8-day at the 9 grassland sites. The shaded areas represent drought years.

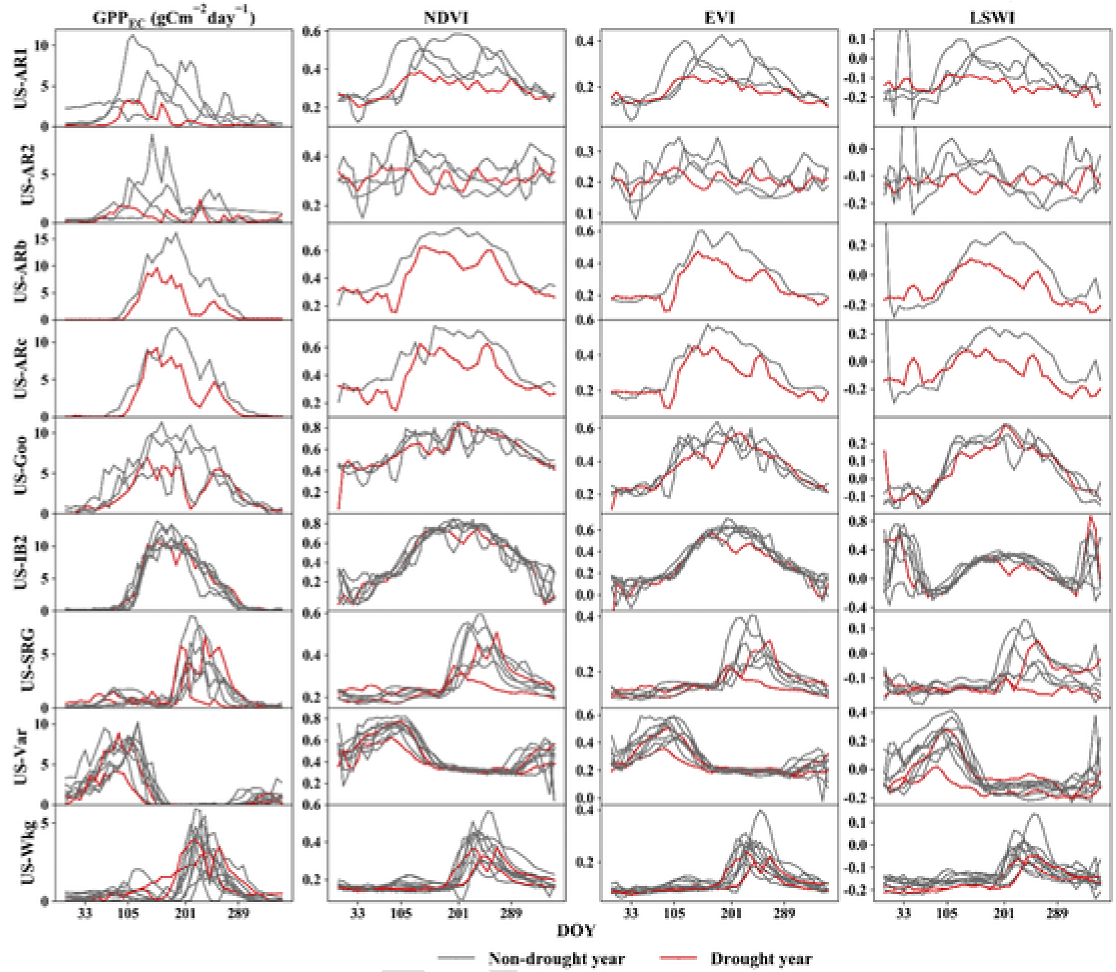


**Fig. 3.** Annual dynamics of $GPP_{EC}$ and remote sensing indices (NDVI, EVI, LSWI) with an interval of 8-day at the 9 grassland sites.

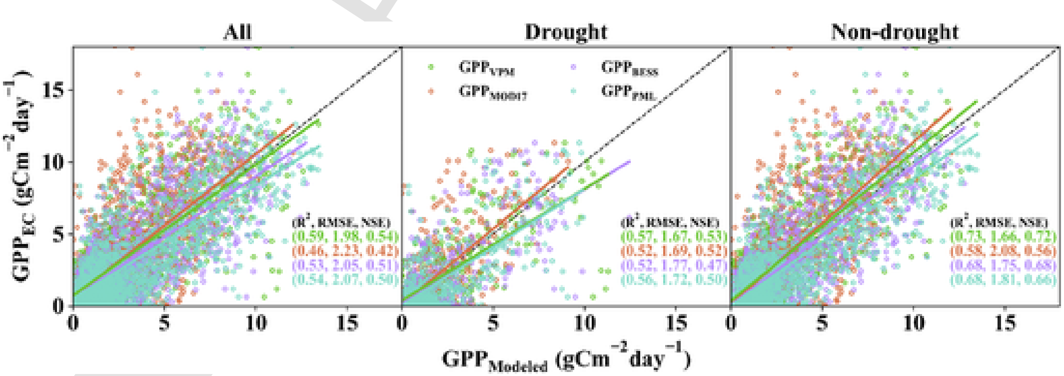


**Fig. 4.** Relationship between gross primary production from the flux tower sites ($GPP_{EC}$) and the predicted GPPs from the four models ($GPP_{VPM}$, $GPP_{BESS}$, $GPP_{MOD17}$, $GPP_{PLM}$) for all the grassland sites in different climate conditions. The unit of RMSE is $gCm^{-2}$ $day^{-1}$.

In summary, the four GPP models performed better in non-drought years than that in drought years. $GPP_{VPM}$ performed best among the four models in all-year, non-drought and drought years, with $R^2$ and NSE higher and RMSE lower than other models. $GPP_{VPM}$ and $GPP_{BESS}$ performed better than $GPP_{PML}$ and $GPP_{MOD17}$ in non-drought years; however, $GPP_{VPM}$ and $GPP_{MOD17}$ performed better than $GPP_{PML}$ and $GPP_{BESS}$ in drought years both in overall and individual sites.

### 3.3. Annual GPP from four GPP products

The annual GPP from flux tower sites and all the four products were calculated in drought and non-drought years.

The bias and RMSE were used to evaluate the performances of the four models in estimating the annual GPP in different conditions.

Overall, the annual GPP estimated from the four models were generally consistent with the annual $GPP_{EC}$. For example, the annual $GPP_{EC}$ was 825 $gCm^{-2}$ $year^{-1}$, and the annual GPP from VPM, MOD17, BESS, and PML were 714 $gCm^{-2}$ $year^{-1}$, 705 $gCm^{-2}$ $year^{-1}$, 854 $gCm^{-2}$ $year^{-1}$, and 940 $gCm^{-2}$ $year^{-1}$ with biases of −13%, −15%, 3%, and 14%, respectively. Although LUE-based GPP models ($GPP_{VPM}$: bias = −17%, and $GPP_{MOD17}$: bias = −16%) performed not as good as process-based GPP models ($GPP_{BESS}$: bias = 1%, and $GPP_{PML}$: bias = 12%) under non-drought years, their performances were better under drought years. $GPP_{VPM}$ slightly overestimated the annual $GPP_{EC}$ with the bias of 2%, and $GPP_{MOD17}$ underestimated annual $GPP_{EC}$ by −10% under drought years. While $GPP_{BESS}$ and $GPP_{PML}$ have substantially overestimated $GPP_{EC}$ by 13% and 21% under drought years. As for individual site, $GPP_{VPM}$ performed best in most of the sites, such as US-AR2, US-ARc, US-Goo, US-SRG, and US-Var, under non-drought years with biased being −17% ~3%. Under drought years, $GPP_{MOD17}$ performed best in US-AR1 (1%), US-AR2 (29%), and US-Goo (13%), while $GPP_{PML}$ performed best in US-ARb (16%), US-ARc (18%), and US-IB2 (10%). In summary, the annual $GPP_{VPM}$ and $GPP_{MOD17}$ performed better than that of $GPP_{BESS}$ and $GPP_{PML}$ in drought years.

## 4. Discussion

### *4.1. Higher GPP accuracy from LUE models than that from process-based models in drought years*

The overall accuracies of these four GPP products (i.e., the MOD17, BESS, VPM, and PML) from this study showed consistencies with that from previous studies in grassland ecosystem and non-drought years (Jiang and Ryu, 2016; Zhang et al., 2017; Zhang et al., 2019b). All the four models showed larger biases (lower $R^2$ and NSE and higher RMSE) in drought years compared to that in non-drought years (Fig. 4). Furthermore, the performances of the four GPP models varied in drought years. In terms of annual GPP, most of the four models have overestimated the $GPP_{EC}$ in drought years, except that $GPP_{MOD17}$ underestimated the $GPP_{EC}$ by −10%. The RMSE of annual GPP between the estimated GPPs and $GPP_{EC}$ were larger in drought years than that in non-drought years for all the models except for the MODIS algorithm.

The LUE models (e.g., VPM and MOD17) performed better in grassland ecosystem than process-based models (e.g., BESS and PML) in drought years (Figs. 4, 5 and 6). Especially for individual site, VPM or MOD17 algorithm performed best in most of the sites (5 out of 9), while PML performed best only in 2 sites (US-IB2 and US-Var) and BESS did not perform best in any of the sites in drought years (Fig. 6). LUE models (i.e., MOD17 and VPM) also achieved better performances than process-based models (e.g., BESS and PML) in the estimation of annual GPP in grassland ecosystem in drought years. The reasons may be attributed to the fact that the LUE models

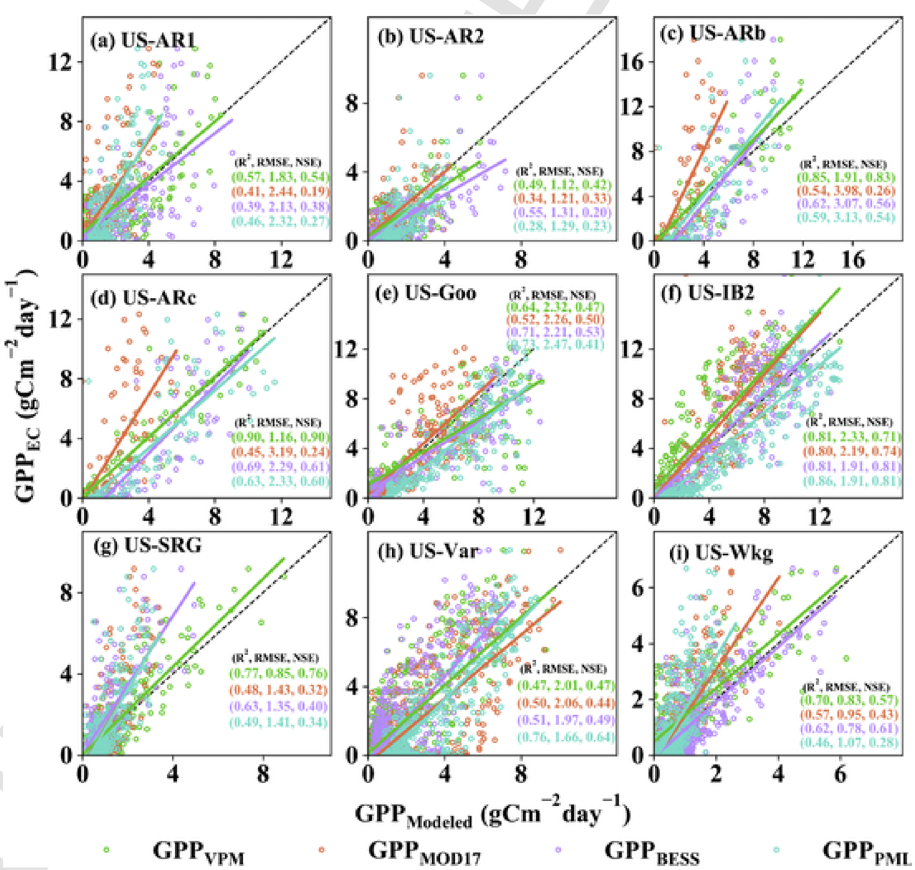


**Fig. 5.** Relationship between gross primary production from the flux tower sites ($GPP_{EC}$) and the predicted GPPs from the four models ($GPP_{VPM}$, $GPP_{BESS}$, $GPP_{MOD17}$, $GPP_{PML}$) for each grassland site. The unit of RMSE is $gCm^{-2}$ $day^{-1}$.

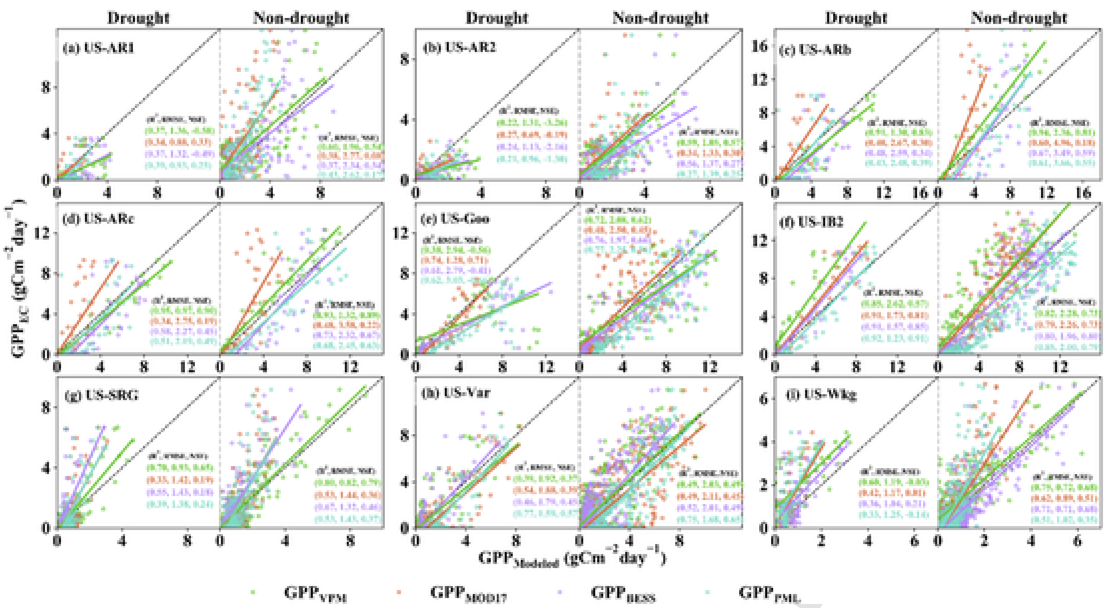


**Fig. 6.** Relationship between gross primary production from the flux tower sites ($GPP_{EC}$) and the predicted GPPs from the four models ($GPP_{VPM}$, $GPP_{BESS}$, $GPP_{MOD17}$, $GPP_{PLM}$) in drought and non-drought years for each grassland site. The unit of RMSE is $gCm^{-2}$ $day^{-1}$.

with simpler model structures have the stronger ability to directly capture the canopy photosynthesis (Dong et al., 2015; Running et al., 2004; Running and Zhao, 2015; Wagle et al., 2015;Xiao et al., 2004a ; Xiao et al., 2004b). While BESS and PML model have complex model structures, which may introduce more uncertainties into GPP estimation (Jiang and Ryu, 2016; Ryu et al., 2011). Previous studies have also reported that the process-based model exhibited larger scattering than LUE model across 10 plant functional types (PFTs), which suggest that LUE models have advantages to simplify complex processes with rather simple structure comparing to process-based model (Alton, 2016). The poor performances by process-based GPP models may be due to the fact that the many parameters used in them have introduced much uncertainties(Alton, 2016), and optimization of these parameters can achieve better model performance.

### 4.2. Model structure and comparison between VPM and MOD17

LUE models estimate GPP as the product of the incident PAR, FPAR and the actual LUE ($\varepsilon$) of vegetation (Monteith, 1972). VPM and MOD17 are both based on LUE concept (Monteith, 1972). However, they have two main differences. Firstly, VPM uses LSWI, which reflects the canopy water content of vegetation, as the water stress factor (Xiao et al., 2004a; Xiao et al., 2004b), while MOD17 algorithm uses VPD, which is an atmospheric moisture indicator, as the water scalar (Running et al., 2004). Under drought conditions, the VPM model performed better in capturing the drought impacts on GPP for grasslands and croplands, and this can be attributed to the higher sensitivity of the land surface water index (i.e., LSWI) (Wagle et al., 2014; Wagle et al., 2015). Previous studies have indicated that, under severe drought conditions, VPD could not capture the variability of water stress on GPP well as it did not explicitly incorporate soil water deficit in canopy gas exchange (Nightingale et al., 2007), such as the underestimation of MOD17 GPP in dry sites in Africa (Sjostrom et al., 2013). By replacing the VPD with a soil water index, the performance of the MOD17 algorithm has been improved largely at the tropical savanna sites in Australia (Kanniah et al., 2009; Leuning et al., 2005). In this study, we compared the relationships between $GPP_{EC}$ and the two $W_{scalar}$s, (i.e. *f*(LSWI) and *f*(VPD)) for individual site, respectively (Fig. 7). *f*(LSWI) had a stronger relationship with $GPP_{EC}$ than *f*(VPD) did for most of the sites (7 out of 9) (Fig. 7), which partly explained the better performance achieved by VPM under drought years, compared to MOD17. This demonstrates that LSWI-based water stress captured the drought effects on GPP better than VPD-based water stress. The better performances of VPM than MOD17 algorithm across various ecosystems, including grassland, under drought or non-drought conditions, have also been demonstrated in previous studies (Doughty et al., 2018; Liu et al., 2014; Wagle et al., 2014; Wagle et al., 2015; Wagle et al., 2016; Wu et al., 2018).

Secondly, VPM uses EVI (chlorophyll or leaf level greenness), while MOD17 algorithm uses canopy level greenness for the estimation of FPAR ($FPAR_{chl}$ vs. $FPAR_{canopy}$) (Running et al., 2004; Running and Zhao, 2015; Xiao et al., 2004a; Xiao et al., 2004b). Previous studies have demonstrated that EVI has a stronger relationship with GPP than does NDVI in various ecosystems (Dong et al., 2015; Jin et al., 2013; Kalfas et al., 2011; Peng et al., 2013; Wagle et al., 2014; Wu et al., 2010). In this study, the relationships between $GPP_{EC}$ and the two FPAR (i.e., $FPAR_{chl}$ and $FPAR_{canopy}$) were further evaluated under drought and non-drought years (Fig. 8). The $FPAR_{chl}$ also showed higher correlation with $GPP_{EC}$ than $FPAR_{canopy}$ did. For example, $FPAR_{chl}$ had a stronger relationship with $GPP_{EC}$ than $FPAR_{canopy}$ did for most of the sites (8 out of 9). $FPAR_{chl}$ also explained 39%~89% (39%~91%) for $GPP_{EC}$, while $FPAR_{canopy}$ only explained 12%~83% (16%~80%) for $GPP_{EC}$ under drought (non-drought) years.

### 4.3. Model structure and comparison between BESS and PML

Process-based GPP models represent the atmosphere-vegetation-soil system as an organic integration, so they can pro-

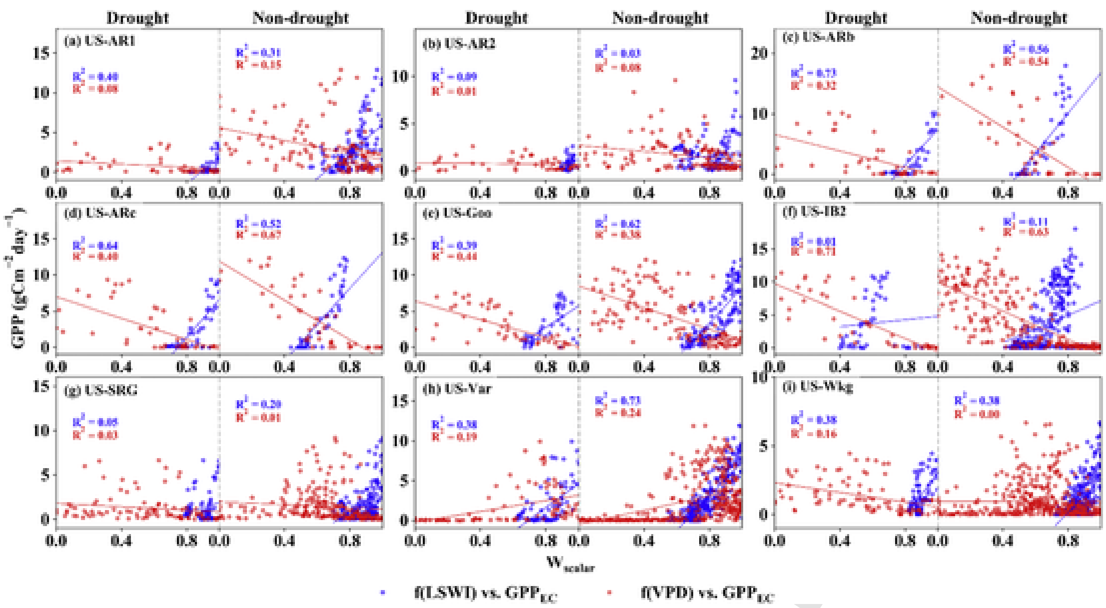


**Fig. 7.** The relationships between $GPP_{EC}$ and the two $W_{scalar}$s (*f*(LSWI), *f*(VPD)) in drought and non-drought years.

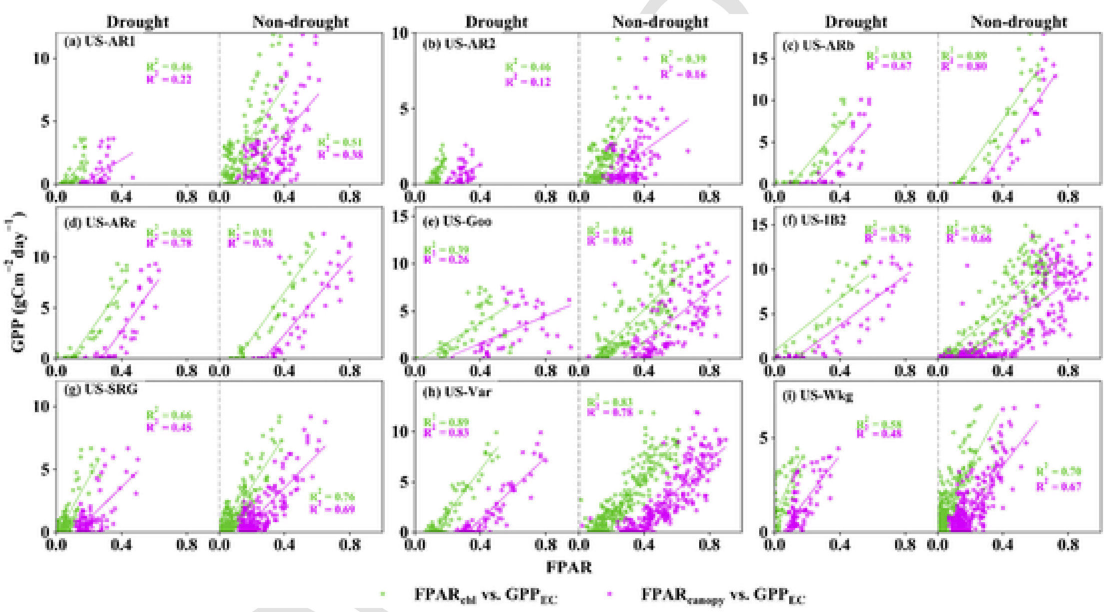


**Fig. 8.** The relationships between $GPP_{EC}$ and the two FPARs ($FPAR_{chl}$, $FPAR_{canopy}$) under drought and non-drought years.

vide deeper insights into the underlying interaction mechanisms of the system (Dickinson, 1983; Jiang and Ryu, 2016; Sellers et al., 1997). BESS and PML belong to the process-based GPP models, both of which coupled with an ET estimation model (Jiang and Ryu, 2016; Ryu et al., 2011; Zhang et al., 2019b). BESS uses relative humidity of the air via the Ball-Berry model to consider the water stress effect on canopy conductance (Ball, 1988; Ryu et al., 2011). In addition, although BESS does not explicitly include a soil moisture effect, it assumes that the soil moisture stress is reflected in the seasonal pattern of leaf area index (LAI), making it better capturing the seasonal water-limiting effects in most seasonally dry ecosystems (Ryu et al., 2011). For example, BESS GPP showed high $R^2$ (>0.6) and low RMSE (0.7 gCm$^{-2}$ day$^{-1}$) for the dry wood savanna flux site (e.g., US-SRM) (Ryu et al., 2011). However, this assumption determines that the performance of BESS GPP under water-limited conditions largely depends on the accuracy of LAI product.

In this study, BESS has a general better performance than PML in non-drought years; however, its accuracy were slightly lower than that of PML in drought years, with higher $R^2$ (0.56 for PML vs. 0.52 for BESS) and NSE (0.50 for PML vs. 0.47 for BESS) and lower RMSE (1.72 gCm$^{-2}$ day$^{-1}$ for PML vs. 1.77 gCm$^{-2}$ day$^{-1}$ for BESS). This may be partly due to the fact that the relative humidity alone used in the BESS model is not a good indicator of atmospheric moisture condition and it also depends on the temperature. For example, a high relative humidity may indicate "dryness" at high temperatures, whereas a low relative humidity may indicate "wetness" at low temperatures (Anderson, 1936; Tack et al., 2015). In addition, BESS uses a fixed ratio between internal leaf and ambient $CO_2$ concentration to avoid the dependence of GPP to VPD, which may also decrease the accuracy of GPP estimation in drought conditions (Jiang and Ryu, 2016; Ryu et al., 2011; Stocker et al., 2019). Compared with relative humidity, the VPD used in the PML model describes the relationship between the actual water vapor pressure and the water vapor pressure at saturation for the same condition, including temperature (Yuan et al., 2019). VPD is a direct indicator of atmospheric moisture status, with high atmosphere VPD usually indicating the atmospheric drought (Yuan et al., 2019; Zhou et al., 2019). Therefore, VPD, the crucial driver of the atmospheric moisture demand for vegetation, has been identified as one of the important constraints on terrestrial ecosystem productivity under drought conditions (Yuan et al., 2019; Zhou et al., 2019). The PML model was first developed for estimating terrestrial evapotranspiration (ET), i.e., PML (Leuning et al., 2008) and PML-V1 (Zhang et al., 2016a). In the version of this study, i.e., PML—V2, a biophysical canopy conductance ($G_c$) model was used to couple the GPP with ET, and it has been successfully tested against GPP observations at 9 eddy-covariance sites including 5 ecosystems in Australia with $R^2 = 0.75$ and RMSE = 1.14 μ mol $m^{-2}$ $s^{-1}$, respectively (Gan et al., 2018). Zhang et al. (2019b) has further improved the PML-V2 by incorporating the VPD to constrain GPP under drought conditions. The water constraint factor based on VPD used in the PML may be explained the better performance of PML than BESS under drought conditions in this study.

### 4.4. Implications for future model improvements

Grassland ecosystems are more susceptible to droughts since they have less accessibility to soil water with shallower roots and higher turnover rates (Frank et al., 2015; Wu et al., 2018). Droughts induce stomatal closure, change of leaf area and angle, and photosynthesis disruption, all of which reduce carbon uptake (Doughty et al., 2018; Li et al., 2019; Wolf et al., 2016; Wu et al., 2018; Yu et al., 2017). When drought takes place in terrestrial ecosystem, photosynthesis is affected by stomatal closure caused by limited water content in leaf and canopy or high VPD in atmosphere (Dong et al., 2015). Therefore, it is critical to capture the process of the stomatal closure and photosynthesis disruption, by using indirect surrogate or direct observation. The VPD is an atmospheric moisture indicator, which can reflect the atmosphere drought condition and to some extent, can further reflect the vegetation responses to droughts, because high VPD could reduce the stomatal conductance and then cause GPP decrease in dry ecosystems. However, because stomatal conductance has a strong control on intercellular $CO_2$ concentration and they have a hyperbolic relationship (Farquhar and Wong, 1984), the reduction of stomatal conductance caused by increasing VPD may have no influence on the rate of photosynthesis at the beginning due to the fact that atmospheric has an adequate supply of $CO_2$ (Zhang et al., 2019a). Soil moisture was first controlled by atmospheric water conditions and soil composition characteristics and thus regulate plant water activity (Geruo et al., 2017; Huang et al., 2016). Some recent studies suggest soil moisture is crucial for monitoring drought impacts on vegetation (Stocker et al., 2019). Stocker et al. (2019) demonstrated that the global GPP reduced by 15% due to soil moisture stress. However, the reliable soil moisture data with global coverage are not available now (Stocker et al., 2019). The soil moisture data used in Stocker et al. (2019) came from the hydrological model simulation. Emerging soil moisture data products derived from microwave remote sensing may provide an improved solution. However, they can only represent the moisture status in upper soil layers, which limit their application in deep-rooted vegetation (Stocker et al., 2019). Based on satellite observations of surface reflectance, LSWI, acting as a plant moisture indicator, can directly reflect the overall water content of leaf, plant stand and soil background in near-real time. The drought status in atmosphere and/or soil will be eventually reflected in vegetation. It is vegetation itself that has the most intuitive and direct response to drought. To understand the mechanistic of plant's responses to drought, it is critical to explore the plant-available water for the reason that it's the actual water pool that plant can get to support transpiration (Huang et al., 2016). Zhang et al. (2015) indicated that the strengths of association between moisture indicators on LUE were ranked as plant indicator (LSWI) > atmospheric indicator (VPD) > soil indicator (soil water content, SWC) for all biomes (Zhang et al., 2015). Our study also suggested that an explicit water stress factor can help the GPP models to achieve better performances under drought conditions. The best performances achieved by VPM under drought years could be attributed to the use of such a drought-sensitive index, i.e., LSWI. LSWI reflected the leaf water content, which can directly represent the responses of vegetation itself to drought. Therefore, to rectify the drought-induced bias in GPP estimations, more efforts should be made in using the water constraint stress factors which directly reflected the vegetation moisture or a comprehensive measurement of vegetation moisture and greenness, such as solar-induced fluorescence.

## 5. Conclusions

Based on 51 site-years observation data derived from 9 grassland flux tower sites, we evaluated the performances of the four state-of-the-art global GPP products (e.g., the MOD17, BESS, VPM, and PML GPP products) under both drought and non-drought years. Correlation analysis between $GPP_{EC}$ and modeled GPPs indicated that all the four models had decreased accuracies under drought years than that under non-drought years. In drought years, VPM was more robust than the MOD17, BESS, and PML models. The varied performances in drought years could be attributed to the differences in representing the water stress effects. The water constraint factor used in VPM was based on LSWI and reflected the leaf water content, which could better capture the vegetation response to drought than that used in MOD17, PML and BESS, all of which used an atmospheric moisture related indicator (the VPD for MOD17 and PML, and the RH for BESS). This study implies that water stress factors which reflected the physiological and ecological characteristics of vegetation itself should be further considered in GPP models to rectify the biases caused by drought and achieve better performance in global terrestrial ecosystem GPP estimation in the context of climate change and increasing extreme climate events.

## Acknowledgement

This study is funded by the Strategic Priority Research Program (XDA19040301) of Chinese Academy of Sciences (CAS). We thank Dr. Youngryel Ryu for the valuable comments during the study. We acknowledge the Data Portal serving the FLUXNET community for making the FLUXNET data available (https://fluxnet.fluxdata.org/data/fluxnet2015-dataset/). We thank the Environmental Ecology Lab in Seoul National University for providing the BESS GPP dataset (http://environment.snu.ac.kr/bess/).

## References


Alton, P.B., 2016. The sensitivity of models of gross primary productivity to meteorological and leaf area forcing: a comparison between a penman-Monteith ecophysiological approach and the MODIS light-use efficiency algorithm. Agric. For. Meteorol. 218, 11–24.

Anderson, D.B., 1936. Relative humidity of vapor pressure deficit. Ecology 17, 277–282.

Angert, A., Biraud, S., Bonfils, C., Henning, C.C., Buermann, W., Pinzon, J., Tucker, C.J., Fung, I., 2005. Drier summers cancel out the CO2 uptake enhancement induced by warmer springs. Proc. Natl. Acad. Sci. U. S. A. 102, 10823–10827.

Baldocchi, D., Penuelas, J., 2019. The physics and ecology of mining carbon dioxide from the atmosphere by ecosystems. Glob. Chang. Biol. 25, 1191–1197.

Baldocchi, D., Falge, E., Gu, L.H., Olson, R., Hollinger, D., Running, S., Anthoni, P., Bernhofer, C., Davis, K., Evans, R., Fuentes, J., Goldstein, A., Katul, G., Law, B., Lee, X.H., Malhi, Y., Meyers, T., Munger, W., Oechel, W.U.K.T.P., Pilegaard, K., Schmid, H.P., Valentini, R., Verma, S., Vesala, T., Wilson, K., Wofsy, S., 2001. FLUXNET: A new tool to study the temporal and spatial variability of ecosystem-scale carbon dioxide, water vapor, and energy flux densities. Bull. Am. Meteorol. Soc. 82, 2415–2434.

Ball, J.T., 1988. An analysis of stomatal conductance. In: Stanford Univ. Stanford Univ, Palo Alto, Calif.

Beer, C., Reichstein, M., Tomelleri, E., Ciais, P., Jung, M., Carvalhais, N., Roedenbeck, C., Arain, M.A., Baldocchi, D., Bonan, G.B., Bondeau, A., Cescatti, A., Lasslop, G., Lindroth, A., Lomas, M., Luyssaert, S., Margolis, H., Oleson, K.W., Roupsard, O., Veenendaal, E., Viovy, N., Williams, C., Woodward, F.I., Papale, D., 2010. Terrestrial gross carbon dioxide uptake: global distribution and covariation with climate. Science 329, 834–838.

Bhattarai, N., Mallick, K., Brunsell, N.A., Sun, G., Jain, M., 2018. Regional evapotranspiration from an image-based implementation of the surface temperature initiated closure (STIC1.2) model and its validation across an aridity gradient in the conterminous US. Hydrol. Earth Syst. Sci. 22, 2311–2341.

Chen, M., Rafique, R., Asrar, G.R., Bond-Lamberty, B., Ciais, P., Zhao, F., Reyer, C.P.O., Ostberg, S., Chang, J., Ito, A., Yang, J., Zeng, N., Kalnay, E., West, T., Leng, G., Francois, L., Munhoven, G., Henrot, A., Tian, H., Pan, S., Nishina, K., Viovy, N., Morfopoulos, C., Betts, R., Schaphoff, S., Steinkamp, J., Hickler, T., 2017. Regional contribution to variability and trends of global gross primary productivity. Environ. Res. Lett. 12.

Chu, H., Baldocchi, D.D., Poindexter, C., Abraha, M., Desai, A.R., Bohrer, G., Arain, M.A., Griffis, T., Blanken, P.D., O'Halloran, T.L., Thomas, R.Q., Zhang, Q., Burns, S.P., Frank, J.M., Christian, D., Brown, S., Black, T.A., Gough, C.M., Law, B.E., Lee, X., Chen, J., Reed, D.E., Massman, W.J., Clark, K., Hatfield, J., Prueger, J., Bracho, R., Baker, J.M., Martin, T.A., 2018. Temporal dynamics of aerodynamic canopy height derived from Eddy covariance momentum flux data across north American flux networks. Geophys. Res. Lett. 45, 9275–9287.

Collatz, G.J., Ribas-Carbo, M., Berry, J.A., 1992. Coupled photosynthesis-stomatal conductance model for leaves of C4 plants. Aust. J. Plant Physiol. 19, 519–538.

Coops, N.C., Black, T.A., Jassal, R.P.S., Trofymow, J.A.T., Morgenstern, K., 2007. Comparison of MODIS, eddy covariance determined and physiologically modelled gross primary production (GPP) in a Douglas-fir forest stand. Remote Sens. Environ. 107, 385–401.

Cote, J.-F., Fournier, R.A., Luther, J.E., van Lier, O.R., 2018. Fine-scale three-dimensional modeling of boreal forest plots to improve forest characterization with remote sensing. Remote Sens. Environ. 219, 99–114.

Dickinson, R.E., 1983. Land surface processes and climate surface albedos and energy-balance. Adv. Geophys. 25, 305–353.

Dong, J., Xiao, X., Wagle, P., Zhang, G., Zhou, Y., Jin, C., Torn, M.S., Meyers, T.P., Suyker, A.E., Wang, J., Yan, H., Biradar, C., Moore, B., III, 2015. Comparison of four EVI-based models for estimating gross primary production of maize and soybean croplands and tallgrass prairie under severe drought. Remote Sens. Environ. 162, 154–168.

Doughty, R., Xiao, X., Wu, X., Zhang, Y., Bajgain, R., Zhou, Y., Qin, Y., Zou, Z., McCarthy, H., Friedman, J., Wagle, P., Basara, J., Steiner, J., 2018. Responses of gross primary production of grasslands and croplands under drought, pluvial, and irrigation conditions during 2010-2016, Oklahoma, USA. Agric. Water Manag. 204, 47–59.

Farquhar, G.D., Wong, S.C., 1984. An empirical-model of stomatal conductance. Aust. J. Plant Physiol. 11, 191–209.

Farquhar, G.D., Caemmerer, S.V., Berry, J.A., 1980. A biochemical-model of photosynthetic CO2 assimilation in leaves of C-3 species. Planta 149, 78–90.

Fischer, M.L., Torn, M.S., Billesbach, D.P., Doyle, G., Northup, B., Biraud, S.C., 2012. Carbon, water, and heat flux responses to experimental burning and drought in a tallgrass prairie. Agric. For. Meteorol. 166, 169–174.

Frank, D., Reichstein, M., Bahn, M., Thonicke, K., Frank, D., Mahecha, M.D., Smith, P., Van der Velde, M., Vicca, S., Babst, F., Beer, C., Buchmann, N., Canadell, J.G., Ciais, P., Cramer, W., Ibrom, A., Miglietta, F., Poulter, B., Rammig, A., Seneviratne, S.I., Walz, A., Wattenbach, M., Zavala, M.A., Zscheischler, J., 2015. Effects of climate extremes on the terrestrial carbon cycle: concepts, processes and potential future impacts. Glob. Chang. Biol. 21, 2861–2880.

Gan, R., Zhang, Y., Shi, H., Yang, Y., Eamus, D., Cheng, L., Chiew, F.H.S., Yu, Q., 2018. Use of satellite leaf area index estimating evapotranspiration and gross assimilation for Australian ecosystems. Ecohydrology 11.

Geruo, A., Velicogna, I., Kimball, J.S., Du, J., Kim, Y., Njoku, E., 2017. Satellite-observed changes in vegetation sensitivities to surface soil moisture and total water storage variations since the 2011 Texas drought. Environ. Res. Lett. 12.

He, B., Liu, J., Guo, L., Wu, X., Xie, X., Zhang, Y., Chen, C., Zhong, Z., Chen, Z., 2018. Recovery of ecosystem carbon and energy fluxes from the 2003 drought in Europe and the 2012 drought in the United States. Geophys. Res. Lett. 45, 4879–4888.

Hoover, D.L., Rogers, B.M., 2016. Not all droughts are created equal: the impacts of interannual drought pattern and magnitude on grassland carbon cycling. Glob. Chang. Biol. 22, 1809–1820.

Huang, Y., Gerber, S., Huang, T., Lichstein, J.W., 2016. Evaluating the drought response of CMIP5 models using global gross primary productivity, leaf area, precipitation, and soil moisture data. Glob. Biogeochem. Cycles 30, 1827–1846.

Jiang, C., Ryu, Y., 2016. Multi-scale evaluation of global gross primary productivity and evapotranspiration products derived from breathing earth system simulator (BESS). Remote Sens. Environ. 186, 528–547.

Jin, C., Xiao, X., Merbold, L., Arneth, A., Veenendaal, E., Kutsch, W.L., 2013. Phenology and gross primary production of two dominant savanna woodland ecosystems in southern Africa. Remote Sens. Environ. 135, 189–201.

Kalfas, J.L., Xiao, X., Vanegas, D.X., Verma, S.B., Suyker, A.E., 2011. Modeling gross primary production of irrigated and rain-fed maize using MODIS imagery and CO2 flux tower data. Agric. For. Meteorol. 151, 1514–1528.

Kanniah, K.D., Beringer, J., Hutley, L.B., Tapper, N.J., Zhu, X., 2009. Evaluation of collections 4 and 5 of the MODIS gross primary productivity product and algorithm improvement at a tropical savanna site in northern Australia. Remote Sens. Environ. 113, 1808–1822.

Leuning, R., Cleugh, H.A., Zegelin, S.J., Hughes, D., 2005. Carbon and water fluxes over a temperate Eucalyptus forest and a tropical wet/dry savanna in Australia: measurements and comparison with MODIS remote sensing estimates. Agric. For. Meteorol. 129, 151–173.

Leuning, R., Zhang, Y.Q., Rajaud, A., Cleugh, H., Tu, K., 2008. A simple surface conductance model to estimate regional evaporation using MODIS leaf area index and the penman-Monteith equation. Water Resour. Res. 44.

Li, X., Li, Y., Chen, A., Gao, M., Slette, I.J., Piao, S., 2019. The impact of the 2009/2010 drought on vegetation growth and terrestrial carbon balance in Southwest China. Agric. For. Meteorol. 269, 239–248.

Liu, Z., Wang, L., Wang, S., 2014. Comparison of different GPP models in China using MODIS image and ChinaFLUX data. Remote Sens. 6, 10215–10231.

Mishra, A.K., Singh, V.P., 2010. A review of drought concepts. J. Hydrol. 391, 204–216.

Monteith, J.L., 1972. Solar-radiation and productivity in tropical ecosystems. J. Appl. Ecol. 9, 747–766.

Naumann, G., Dutra, E., Barbosa, P., Pappenberger, F., Wetterhall, F., Vogt, J.V., 2014. Comparison of drought indicators derived from multiple data sets over Africa. Hydrol. Earth Syst. Sci. 18, 1625–1640.

Nightingale, J.M., Coops, N.C., Waring, R.H., Hargrove, W.W., 2007. Comparison of MODIS gross primary production estimates for forests across the USA with those generated by a simple process model, 3-PGS. Remote Sens. Environ. 109, 500–509.

Peng, Y., Gitelson, A.A., Sakamoto, T., 2013. Remote estimation of gross primary productivity in crops using MODIS 250 m data. Remote Sens. Environ. 128, 186–196.

Potop, V., Boroneanţ, C., Možný, M., Štěpánek, P., Skalák, P., 2014. Observed spatiotemporal characteristics of

drought on various time scales over the Czech Republic. Theor. Appl. Climatol. 115, 563–581.
Prabnakorn, S., Maskey, S., Suryadi, F.X., de Fraiture, C., 2018. Rice yield in response to climate trends and drought index in the Mun River Basin, Thailand. Sci. Total Environ. 621, 108–119.
Prince, S.D., Goward, S.N., 1995. Global primary production: a remote sensing approach. J. Biogeogr. 22, 815–835.
Reichstein, M., Falge, E., Baldocchi, D., Papale, D., Aubinet, M., Berbigier, P., Bernhofer, C., Buchmann, N., Gilmanov, T., Granier, A., Grunwald, T., Havrankova, K., Ilvesniemi, H., Janous, D., Knohl, A., Laurila, T., Lohila, A., Loustau, D., Matteucci, G., Meyers, T., Miglietta, F., Ourcival, J.M., Pumpanen, J., Rambal, S., Rotenberg, E., Sanz, M., Tenhunen, J., Seufert, G., Vaccari, F., Vesala, T., Yakir, D., Valentini, R., 2005. On the separation of net ecosystem exchange into assimilation and ecosystem respiration: review and improved algorithm. Glob. Chang. Biol. 11, 1424–1439.
Running, S.W., Zhao, M., 2015. User's Guide Daily GPP and Annual NPP (MOD17A2/A3) Products NASA Earth Observing System MODIS Land Algorithm.
Running, S.W., Nemani, R.R., Heinsch, F.A., Zhao, M.S., Reeves, M., Hashimoto, H., 2004. A continuous satellite-derived measure of global terrestrial primary production. Bioscience 54, 547–560.
Ryu, Y., Baldocchi, D.D., Kobayashi, H., van Ingen, C., Li, J., Black, T.A., Beringer, J., van Gorsel, E., Knohl, A., Law, B.E., Roupsard, O., 2011. Integration of MODIS land and atmosphere products with a coupled-process model to estimate gross primary productivity and evapotranspiration from 1 km to global scales. Glob. Biogeochem. Cycles 25.
Ryu, Y., Jiang, C., Kobayashi, H., Detto, M., 2018. MODIS-derived global land products of shortwave radiation and diffuse and total photosynthetically active radiation at 5 km resolution from 2000. Remote Sens. Environ. 204, 812–825.
Ryu, Y., Berry, J.A., Baldocchi, D.D., 2019. What is global photosynthesis? History, uncertainties and opportunities. Remote Sens. Environ. 223, 95–114.
Schwalm, C.R., Anderegg, W.R.L., Michalak, A.M., Fisher, J.B., Biondi, F., Koch, G., Litvak, M., Ogle, K., Shaw, J.D., Wolf, A., Huntzinger, D.N., Schaefer, K., Cook, R., Wei, Y., Fang, Y., Hayes, D., Huang, M., Jain, A., Tian, H., 2017. Global patterns of drought recovery. Nature 548, 202.
Scott, R.L., Hamerlynck, E.P., Jenerette, G.D., Moran, M.S., Barron-Gafford, G.A., 2010. Carbon dioxide exchange in a semidesert grassland through drought-induced vegetation change. J. Geophys. Res. Biogeosci. 115.
Sellers, P.J., Dickinson, R.E., Randall, D.A., Betts, A.K., Hall, F.G., Berry, J.A., Collatz, G.J., Denning, A.S., Mooney, H.A., Nobre, C.A., Sato, N., Field, C.B., Henderson-Sellers, A., 1997. Modeling the exchanges of energy, water, and carbon between continents and the atmosphere. Science 275, 502–509.
Sjostrom, M., Zhao, M., Archibald, S., Arneth, A., Cappelaere, B., Falk, U., de Grandcourt, A., Hanan, N., Kergoat, L., Kutsch, W., Merbold, L., Mougin, E., Nickless, A., Nouvellon, Y., Scholes, R.J., Veenendaal, E.M., Ardo, J., 2013. Evaluation of MODIS gross primary productivity for Africa using eddy covariance data. Remote Sens. Environ. 131, 275–286.
Stocker, B.D., Zscheischler, J., Keenan, T.F., Prentice, I.C., Seneviratne, S.I., Penuelas, J., 2019. Drought impacts on terrestrial primary production underestimated by satellite monitoring. Nat. Geosci. 12, 264.
Tack, J., Singh, R.K., Nalley, L.L., Viraktamath, B.C., Krishnamurthy, S.L., Lyman, N., Jagadish, K.S.V., 2015. High vapor pressure deficit drives salt-stress-induced rice yield losses in India. Glob. Chang. Biol. 21, 1668–1678.
Um, M.-J., Kim, Y., Park, D., 2018. Evaluation and modification of the drought severity index (DSI) in East Asia. Remote Sens. Environ. 209, 66–76.
Vicente-Serrano, S.M., Begueria, S., Lopez-Moreno, J.I., 2010. A multiscalar drought index sensitive to global warming: the standardized precipitation evapotranspiration index. J. Clim. 23, 1696–1718.
Vicente-Serrano, S.M., Van der Schrier, G., Begueria, S., Azorin-Molina, C., Lopez-Moreno, J.-I., 2015. Contribution of precipitation and reference evapotranspiration to drought indices under different climates. J. Hydrol. 526, 42–54.
Wagle, P., Xiao, X., Torn, M.S., Cook, D.R., Matamala, R., Fischer, M.L., Jin, C., Dong, J., Biradar, C., 2014. Sensitivity of vegetation indices and gross primary production of tallgrass prairie to severe drought. Remote Sens. Environ. 152, 1–14.
Wagle, P., Xiao, X., Suyker, A.E., 2015. Estimation and analysis of gross primary production of soybean under various management practices and drought conditions. ISPRS J. Photogramm. Remote Sens. 99, 70–83.
Wagle, P., Zhang, Y., Jin, C., Xiao, X., 2016. Comparison of solar-induced chlorophyll fluorescence, light-use efficiency, and process-based GPP models in maize. Ecol. Appl. 26, 1211–1222.
Wolf, S., Keenan, T.F., Fisher, J.B., Baldocchi, D.D., Desai, A.R., Richardson, A.D., Scott, R.L., Law, B.E., Litvak, M.E., Brunsell, N.A., Peters, W., van der Laan-Luijkx, I.T., 2016. Warm spring reduced carbon cycle impact of the 2012 US summer drought. Proceed. Nat. Acad. Sci. U.S.A. 113, 5880–5885.
Wu, C., Niu, Z., Gao, S., 2010. Gross primary production estimation from MODIS data with vegetation index and photosynthetically active radiation in maize. J. Geophys. Res.-Atmos. 115.
Wu, X., Xiao, X., Zhang, Y., He, W., Wolf, S., Chen, J., He, M., Gough, C.M., Qin, Y., Zhou, Y., Doughty, R., Blanken, P.D., 2018. Spatiotemporal consistency of four gross primary production products and solar-induced chlorophyll fluorescence in response to climate extremes across CONUS in 2012. J. Geophys. Res. Biogeosci. 123, 3140–3161.
Xiao, X.M., Hollinger, D., Aber, J., Goltz, M., Davidson, E.A., Zhang, Q.Y., Moore, B., 2004. Satellite-based modeling of gross primary production in an evergreen needleleaf forest. Remote Sens. Environ. 89, 519–534.
Xiao, X.M., Zhang, Q.Y., Braswell, B., Urbanski, S., Boles, S., Wofsy, S., Berrien, M., Ojima, D., 2004. Modeling gross primary production of temperate deciduous broadleaf forest using satellite images and climate data. Remote Sens. Environ. 91, 256–270.
Yao, Y., Wang, X., Li, Y., Wang, T., Shen, M., Du, M., He, H., Li, Y., Luo, W., Ma, M., Ma, Y., Tang, Y., Wang, H., Zhang, X., Zhang, Y., Zhao, L., Zhou, G., Piao, S., 2018. Spatiotemporal pattern of gross primary productivity and its covariation with climate in China over the last thirty years. Glob. Chang. Biol. 24, 184–196.
Yu, Z., Wang, J., Liu, S., Rentch, J.S., Sun, P., Lu, C., 2017. Global gross primary productivity and water use efficiency changes under drought stress. Environ. Res. Lett. 12.
Yuan, W., Zheng, Y., Piao, S., Ciais, P., Lombardozzi, D., Wang, Y., Ryu, Y., Chen, G., Dong, W., Hu, Z., Jain, A.K., Jiang, C., Kato, E., Li, S., Lienert, S., Liu, S., Nabel, J.E.M.S., Qin, Z., Quine, T., Sitch, S., Smith, W.K., Wang, F., Wu, C., Xiao, Z., Yang, S., 2019. Increased atmospheric vapor pressure deficit reduces global vegetation growth. Sci. Adv. 5.
Zhang, Y., Leuning, R., Hutley, L.B., Beringer, J., McHugh, I., Walker, J.P., 2010. Using long-term water balances to parameterize surface conductances and calculate evaporation at 0.05 degrees spatial resolution. Water Resour. Res. 46.
Zhang, L., Wylie, B.K., Ji, L., Gilmanov, T.G., Tieszen, L.L., Howard, D.M., 2011. Upscaling carbon fluxes over the Great Plains grasslands: sinks and sources. J. Geophys. Res. Biogeosci. 116.
Zhang, Y., Song, C., Sun, G., Band, L.E., Noormets, A., Zhang, Q., 2015. Understanding moisture stress on light use efficiency across terrestrial ecosystems based on global flux and remote-sensing data. J. Geophys. Res. Biogeosci. 120, 2053–2066.
Zhang, Y., Pena-Arancibia, J.L., McVicar, T.R., Chiew, F.H.S., Vaze, J., Liu, C., Lu, X., Zheng, H., Wang, Y., Liu, Y.Y., Miralles, D.G., Pan, M., 2016. Multi-decadal trends in global terrestrial evapotranspiration and its components. Sci. Rep. 6.
Zhang, Y., Xiao, X., Jin, C., Dong, J., Zhou, S., Wagle, P., Joiner, J., Guanter, L., Zhang, Y., Zhang, G., Qin, Y., Wang, J., Moore, B., III, 2016. Consistency between sun-induced chlorophyll fluorescence and gross primary production of vegetation in North America. Remote Sens. Environ. 183, 154–169.
Zhang, Y., Xiao, X., Zhou, S., Ciais, P., McCarthy, H., Luo, Y., 2016. Canopy and physiological controls of GPP during drought and heat wave. Geophys. Res. Lett. 43, 3325–3333.
Zhang, Y., Xiao, X., Wu, X., Zhou, S., Zhang, G., Qin, Y., Dong, J., 2017. Data descriptor: a global moderate resolution dataset of gross primary production of vegetation for 2000-2016. Sci. Data 4.
Zhang, Q., Ficklin, D.L., Manzoni, S., Wang, L., Way, D., Phillips, R.P., Novick, K.A., 2019. Response of ecosystem intrinsic water use efficiency and gross primary productivity to rising vapor pressure deficit. Environ. Res. Lett. 14.
Zhang, Y., Kong, D., Gan, R., Chiew, F.H.S., McVicar, T.R., Zhang, Q., Yang, Y., 2019. Coupled estimation of 500 m and 8-day resolution global evapotranspiration and gross primary production in 2002-2017. Remote Sens. Environ. 222, 165–182.
Zhao, M.S., Heinsch, F.A., Nemani, R.R., Running, S.W., 2005. Improvements of the MODIS terrestrial gross and net primary production global data set. Remote Sens. Environ. 95, 164–176.
Zhou, S., Williams, A.P., Berg, A.M., Cook, B.I., Zhang, Y., Hagemann, S., Lorenz, R., Seneviratne, S.I., Gentine, P., 2019. Land-atmosphere feedbacks exacerbate concur-

rent soil drought and atmospheric aridity. Proc. Natl. Acad. Sci. U. S. A. 116, 18848–18853.

Zhu, X., Pei, Y., Zheng, Z., Dong, J., Zhang, Y., Wang, J., Chen, L., Doughty, R.B., Zhang, G., Xiao, X., 2018. Underestimates of grassland gross primary production in MODIS standard products. Remote Sens. 10.